Structural Analysis of a Roof Extracted from a Wind Turbine Blade

T. Russell Gentry[1]; Tristan Al-Haddad[2]; Lawrence C. Bank, Dist.M.ASCE[3]; Franco R. Arias[4]; Angela Nagle[5]; and Paul Leahy[6]

Abstract: The objective of this research is to demonstrate that parts of decommissioned wind turbine blades can be repurposed for infrastructure applications for a sustainable future of the wind power industry. The purpose of this paper was to develop a methodology to conduct detailed structural engineering design of composite material parts extracted from wind turbine blades. A large section extracted from a 100-m long blade was repurposed as a roof for a small (approximately 40 m^2) single-story masonry house. Geometric and material properties were taken from the blade design documents. A three-dimensional graphical model was created from the exterior surface and material layups. The roof was designed using the load and resistance factor design method familiar to civil engineers. Analysis of stresses and defections was conducted using hand calculations and the finite element method. The results of the analyses showed that the roof is within code mandated stress and deflection limits. The methodology developed could be applied to other wind blade repurposing concepts.
DOI: 10.1061/(ASCE)AE.1943-5568.0000440.

Author keywords: Recycling; Repurposing; Design; Finite element analysis; Wind turbine blades.

Introduction

Fiber reinforced polymer (FRP) composite materials are not biodegradable and present unique problems for waste management and their end-of-life (EOL). The impact of polymers on the environment and society has become a major concern in many countries. In response to the European Waste Directive (DIRECTIVE 2008/98/EC; Directive 2008), the option of disposing of EOL FRP blades in landfills is now restricted by landfill taxes and reuse, recycling, and recovery targets. Since the 1990s, there has been a developing body of research that has studied the issues of recycling and EOL of FRP composites, in general, and composite wind blades, in particular. Recent analyses of the key issues related to the EOL of wind turbine blades can be found in Liu and Barlow (2017), Jensen and Skelton (2018), and Bank et al. (2018). For example, a typical 2.0 MW turbine with three 50 m blades has approximately 20 tons of FRP material and an 8 MW turbine has approximately 80 tons of FRP material (based on a conservative 1 MW ≈ 10 tons of FRP conversion). Based on a predicted "moderate growth scenario" from the Global Wind Energy Council (GWEC), waste blades from future wind power installations will total of 16.8 million tons by 2030 and 39.8 million tons by 2050 if no action is taken in the interim (GWEC 2016). At the present time, numerous large (40–60 m) composite material wind turbine blades are coming out of service due to their original 20-year design life or due to replacement by more efficient turbines and/or blades (referred to as repowering).

Managing Composite Material "Waste"

There are various methods to manage waste composites (either production waste or EOL waste products) at the present time (Oliveux et al. 2015; Job et al. 2016), some of which are referred to as "recycling." Unfortunately, the term "recycling" has several different meanings in this field and the term "second life" is preferred so there is a clear understanding of their position in a waste processing hierarchy. Following Skelton (2017) and Jensen and Skelton (2018) we propose the following categorization of second-life options for FRP wind blades:

1. **Reuse:** In this scenario the entire blade is reused. The blade is used as a turbine blade in its second life but has its lifetime extended by refurbishment or remanufacturing, or is sold on the second-hand market.
2. **Repurpose:** In this scenario the structural properties and the material properties of the composite are repurposed. The blade is used whole or sectioned into parts and repurposed for other products such as parts of temporary or inexpensive housing, office and home furniture, benches and playgrounds, pedestrian bridges, and powerline structures (Bank et al. 2018; Adamcio 2019; Bladesign 2019; SuperuseStudios 2012; Speksnijder 2018; Suhail et al. 2019; Adamcio 2019; Bank et al. 2019; Alshannaq et al. 2019).

[1]Associate Professor, School of Architecture, Georgia Institute of Technology, 245 4th St. NW, Atlanta, GA 30332. Email: russell.gentry@design.gatech.edu

[2]Lecturer, School of Architecture, Georgia Institute of Technology, 245 4th St. NW, Atlanta, GA 30332. Email: tristan.al-haddad@formations-studio.com

[3]Research Faculty, School of Architecture, Georgia Institute of Technology, 245 4th St. NW, Atlanta, GA 30332 (corresponding author). ORCID: https://orcid.org/0000-0002-4279-4473. Email: larry.bank@design.gatech.edu

[4]Former Graduate Student, Civil Engineering Dept., City College of New York, 160 Convent Av, New York, NY 10031. Email: farias.civeng@gmail.com

[5]Graduate Student, School of Engineering, Structural and Environmental Engineering, Univ. College Cork, College Rd., Cork, Republic of Ireland. Email: angelajanenagle@umail.ucc.ie

[6]Lecturer, School of Engineering, Structural and Environmental Engineering, Univ. College Cork, College Rd., Cork, Republic of Ireland. Email: paul.leahy@ucc.ie

Note. This manuscript was submitted on December 3, 2019; approved on July 27, 2020; published online on September 25, 2020. Discussion period open until February 24, 2021; separate discussions must be submitted for individual papers. This paper is part of the ***Journal of Architectural Engineering***, © ASCE, ISSN 1076-0431.

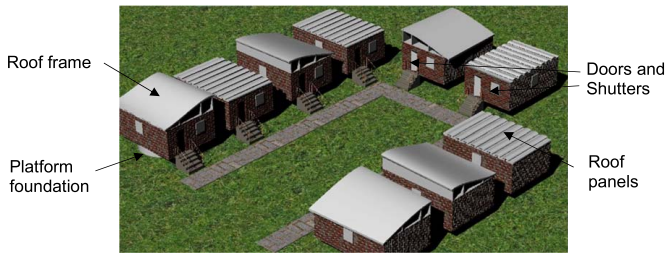

Fig. 1. Repurposing concepts for housing from 100-m long blade parts.

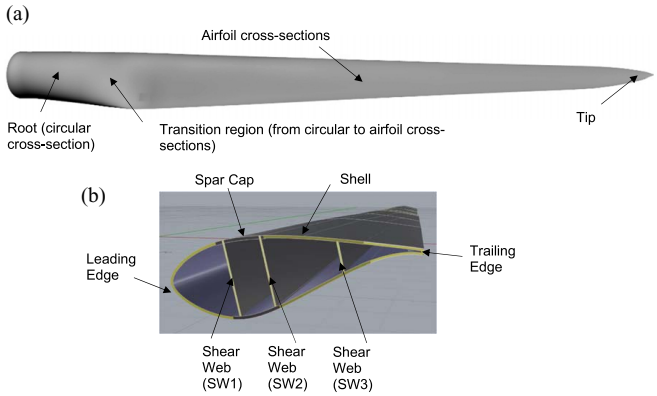

Fig. 2. (a) Entire 100-m long blade; and (b) cross-sectional view at Station 19 (27.6 m from the root end).

3. **Recycle**
   a. **Fully-recycle:** In this scenario the material properties of the composite are recycled. The blade is cut, shred, or ground into small pieces or granular material as filler for use in concrete or other composites (Beauson et al. 2016; Mamanpush et al. 2018; Yazdanbakhsh et al. 2018; Rodin et al. 2018).
   b. **Partially-recycle:** In this scenario the glass fiber constituent of the composite is used. This includes thermo–chemical methods such as pyrolysis, solvolysis, and thermolysis (fluidized bed) (Oliveux et al. 2015) that are used to reclaim the glass fiber. Or the glass fiber is used as a feedstock for cement clinker by coprocessing the shredded composite material in a cement kiln (Ramesh et al. 2018).

Waste disposal methods such as landfilling or incineration, with or without energy recovery, or syngas production are not considered to be second-life methods since no material is reused in a new product. Clearly, all the second-life methods listed will need "third-life" or other disposal methods in the future. In most of the world landfilling is the predominant method of disposing of FRP scrap and EOL waste costing in the range of $45–200 per ton. With increased awareness of the environmental impacts of climate change, decreased and more expensive natural resources, and greater global concerns for health, the barriers to FRP production and waste disposal are likely to increase.

In what follows, the repurposing of a part extracted from a 100-m long FRP blade as a roof structure is discussed. Fig. 1 shows conceptual designs for platform foundations, doors, window shutters, roof panels, and roofs for small (approx. 40 m^2) masonry block houses (Bank et al. 2018). Such buildings are ubiquitous in the developing world. Of the different possible uses of the blade parts shown in Fig. 1, the roof was chosen for further detailed structural analysis because of its large size and complex geometry and materials. The study follows and expands a prior conceptual study of a similar roof structure with different geometry and calculations (Bank et al. 2019).

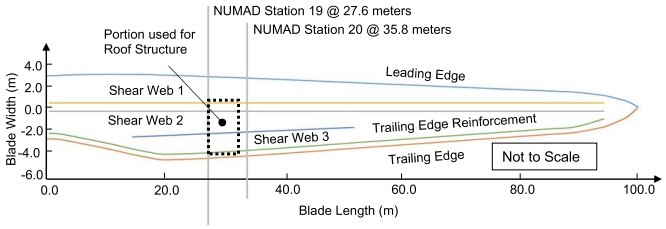

Fig. 3. Location of roof section extracted from blade (along the length).

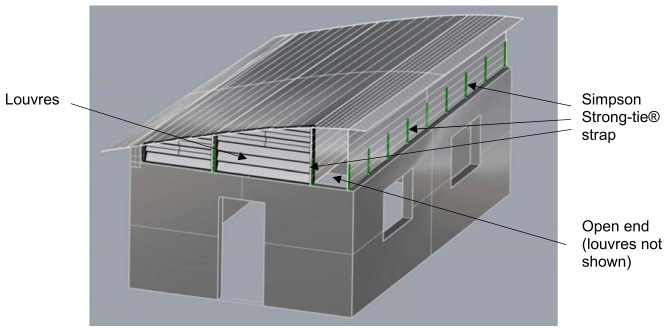

Fig. 4. Schematic of roof.

Wind Blade Geometry

The wind blade selected for the current work was a 100-m long prototype wind blade designed by Sandia National Laboratories (SNL) identified as SNL-100-01 (Griffith 2013). This blade is similar in size to the 107-m turbine blade currently being manufactured for a 12 MW turbine (General Electric 2019). The geometry is defined by 25 different airfoils at specific stations along the blade length from the root end, where the blade is connected to the turbine hub, to the tip. The materials are defined by 393 different solid and sandwich composite material layups. The SNL-100-01 model of the blade is a two-dimensional wire frame (surface) model built using the Numerical Manufacturing and Design Tool (NuMAD) (Berg and Resor 2012; Arias 2016). A three-dimensional (3-D) architectural model of the blade including thickness and material types at all locations is required for architectural and structural calculations and detailing. Fig. 2 shows the 3-D model of the 100-m blade that was built from the stack layups and material types provided in Griffith (2013) using Rhinoceros 3D (version 5.0, Robert McNeel & Associates, Washington; Arias 2017).

The blade has a maximum chord (i.e., the distance between the leading and trailing edges) of 7.628 m at a distance of 19.5 m from the root end. The blade has a foam core shell, three internal foam core webs [identified as SW1, SW2, and SW3 from left to right in Fig. 2(b)] and a carbon fiber spar cap (shown in black above and below the webs SW1 and SW2). The part of the 100-m blade that was extracted from the 3-D blade model to create the roof region was extracted from Station 19 to Station 20 (27.6–35.8 m) and is shown schematically in Fig. 3.

A schematic rendering of the part used for the roof is shown on the masonry block walls of the approximately 40 m^2 house in Fig. 4. Fig. 4 also shows schematics of the connection details using Simpson Strong-Tie straps between the blade roof and the masonry walls; and schematics of louver-type window shades to enclose the open ends of the blade roof. Louver-type windows and shades are commonly used in informal housing in developing

countries where high humidity and temperatures are common (Bank et al. 2018).

Structural Analysis of the Roof

Dimensions

The center-line dimensions of the roof used in the calculations that follow are shown in Fig. 5.

Materials

The mechanical and physical properties of the materials as well as their layups in different locations around the cross section and along the length of the SNL-100-01 blade are given in Griffith (2013). These are based on the MSU material test database (Mandell and Samborsky 1997; SNL 2019). In cases where properties were not provided in Griffith (2013) they were obtained from the literature as noted in Table 1.

The geometric and material properties of the roof were determined for the laminates and sandwich panels for the region from Station 19 to Station 20 (27.6–35.8 m). These were used in both hand calculations and in the LS-DYNA finite element method (FEM) analysis in what follows. The as-reported properties given in Griffith were used in the analysis. Any changes in material properties or dimensions due to the expected 20-year in-service operation of the blade were not considered at this time. The estimation of residual properties in wind blades after 20 years of service (known as remaining-life) is an active research field (Post et al. 2010).

Design Philosophy

For civil engineering structural analysis of composite material structures, the load and resistance factor design (LRFD; or its equivalent called limit state design in the EU) methods or allowable stress design methods are used (Bank 2006). The two primary limit states analyzed are the ultimate limit state (ULS) and the serviceability limit state (SLS). In the ULS (strength, stability) analysis, nominal service loads are typically increased using prescribed load factors, and the structural or material capacities are typically reduced using prescribed resistance or materials safety factors. In the SLS (e.g., deflections, vibrations), neither the nominal service loads nor the material properties are typically factored. The loads for the ULS and SLS are referred to as the factored loads or the service loads, respectively.

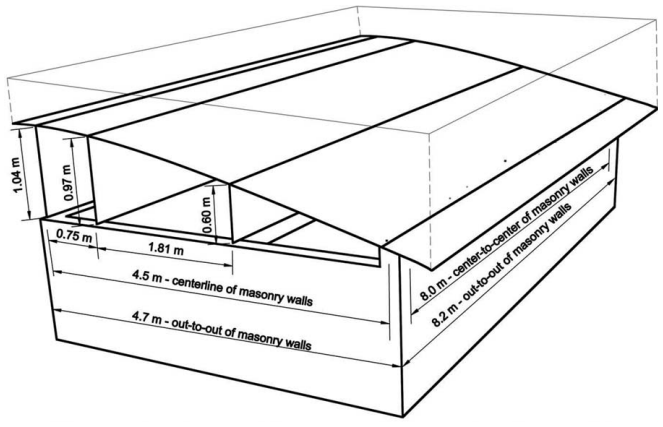

Fig. 5. Dimensions of the roof (perspective drawing).

Nominal service live loads and load combinations (load cases) are used for a civil engineering structural design and are stipulated in ASCE 7-16 (ASCE 2016) or Eurocode EN 1991: Actions on structures (CEN 1991). Load combinations are factored amounts of nominal dead load, live load, roof live load, wind load, snow load, and others (ASCE 7-16).

The resistance or material factors depend on the type of materials used and are given in separate material-specific design codes (e.g., for concrete, ACI 318-19 (ACI 2019) or EN 1992: Design of concrete structures (CEN 1992). At the time of writing, an approved design code does not exist for composite materials for civil engineering structures. An ASCE standard and a Eurocode are currently under development. In the absence of a code, the material factors for the FRP materials used in this analysis were taken from Ascione et al. (2016), the precursor document to the Eurocode. The material partial factor, γ_M, for ultimate strength was calculated to be $\gamma_M = (1.15 \times 1.35 \times 1.2) = 1.86$, assuming (1) the material properties were obtained by test ($\gamma_{M1} = 1.15$), (2) the production processes and properties of the materials have a standard deviation ≤ 0.10 ($\gamma_{M2} = 1.35$), and (3) the material was not postcured ($\gamma_{M3} = 1.2$).

For the serviceability analysis the nominal service loads were used and the material partial factor, $\gamma_M = 1.0$. For most structures the serviceability requirements are set by building codes [e.g., International Building Code (ICC 2018)]. For roof structures the requirement is typically that the deflection, δ, (displacement downward due to gravity) be $\delta < L/240$ (i.e., the member span divided by 240).

It is also of interest to note that design codes for composite wind blades themselves are not yet available. Technical committee TC 88, working group PT 61400-5 of the International Electrotechnical Commission (IEC) is currently working on IEC 61400—Part 5: Rotor blades. However, even when these codes are published, they will not be suitable for structural design for civil structures since local authorities provide construction permits for projects based on building codes such as the International Building Code (ICC 2018), which incorporate the model material design codes (e.g., ACI-318).

Loads for Roof Design

For the purposes of the proof-of-principle analysis presented in this paper only one load combination was considered: dead load + roof live load ($D + L_r$). Only a uniform dead load was considered. Concentrated live load, wind, snow, or ice load on the roof load were not considered at this time. This was done to demonstrate the methodology needed for such calculations. It is important to note that other load cases, especially those related to wind loads, also need to be analyzed. Wind load can create uplift on a roof system that could affect not only the design of the roof itself but, perhaps more significantly, the design of the connection details and louvers, shown in Fig. 4.

The dead load was determined by uniformly distributing the entire 24.32 kN weight of the roof (determined from the material densities and volumes) over the entire projected roof area of 42.9 m^2. This gave a uniformly distributed dead load, $D = 0.566$ kN/m^2. The code-stipulated roof live load, $L_r = 0.96$ kN/m^2, was used. This gives an unfactored service load of 1.52 kN/m^2 and a factored load of $1.2(0.566) + 1.6(0.96) = 2.212$ kN/m^2 (ASCE 7-16 LRFD load combination 3).

Preliminary Analysis—Hand Calculations

Hand calculations using one-dimensional mechanics-of-materials models were used to determine stresses in individual elements of the roof: Case 1, the shell panel between the second shear web

Table 1. Material properties of laminates in the SNL-100-01

Material type	E_{11} (GPa)	E_{22} (GPa)	G_{12} (GPa)	ν_{12}	ρ (kg/m^3)	$\sigma_{11(tens)}$ (MPa)	$\sigma_{11(comp)}$ (MPa)	$\sigma_{22(tens)}$ (MPa)	$\sigma_{22(comp)}$ (MPa)	τ (MPa)
Foam	0.256	0.256	0.022	0.3	200	3.1[a]	−3.8[a]	3.1[a]	−3.8[a]	2.0[a]
Glass UD $[0]_2$	41.80	14.00	2.63	0.28	1,920	972	−702	31[b]	−118[b]	72[b]
SNLBiax $[\pm45]_4$	13.60	13.30	11.80	0.51	1,780	144	−213	144	−213	—
SNLTriax $[\pm45]_4[0]_2$	27.70	13.65	7.20	0.39	1,850	972	−702	144[c]	−213[c]	—
SNLCarbon (UD)	114.50	8.39	5.99	0.27	1,220	1,546	−1,047	52[b]	−206[b]	93[b]

Note: — = not determined (not used in analysis).
[a]From AIREX T92.200 (3A Core Materials 2018).
[b]From Agarwal et al. (2006).
[c]Assumes that ±45 plies control strength in transverse direction.

and the trailing edge, and Case 2, the third shear web of the roof section. These two cases were chosen for the hand calculations since they were found to be those that gave the largest local deflections and stresses in the roof structure based on a prior approximate analysis conducted (Bank et al. 2019). Simplifying assumptions were made relative to the boundary conditions of the shell and web sandwich panels in order to obtain a rough order of magnitude estimate of the stresses prior to conducting the detailed FEM analysis described in the following section. Such analyses are routinely made in the early conceptual design stages by structural engineers and architects.

Out-of-Plane Bending of the Shell Panel

The sandwich panel at the chosen location in the blade consists of a 60-mm thick thermoplastic foam core and two 5 mm composite material face skins of SNLTriax (Table 1). Since this shell panel is in the transverse (contour) orientation relative to the blade (and roof) longitudinal axis, the transverse stiffness and strength properties of the materials were used: $E_{22(Triax)} = 13.65$ GPa, $E_{foam} = 0.256$ GPa, $\sigma_{22(Triax)} = +144$ MPa, $\sigma_{22(Triax)} = -213$ MPa, $\sigma_{tens(foam)} = +3.1$ MPa, $\sigma_{comp(foam)} = -3.8$ MPa, and $\tau_{ult(foam)} = 2.0$ MPa (Table 1).

The shear web sandwich panels consist of a 60-mm thick thermoplastic foam core and two 3 mm composite material face skins of SNLBiax (Table 1). Since the shear web sandwich panels are parallel to the blade (and roof) longitudinal axis, the longitudinal stiffness and strength properties of the materials were used: $E_{11(biax)} = 13.60$ GPa, $E_{foam} = 0.256$ GPa, $\sigma_{11(Biax)} = +144$ MPa, and $\sigma_{11(Biax)} = -213$ MPa.

The critical shell panel for analysis was assumed to span between the second web and the trailing edge over the third web as shown in Fig. 6. It was analyzed as a flat continuous beam of unit-width 1 m, over three supports (S1, S2, and S3): S1 second web (0.9 m), S2 third web (0.6 m), and S3 the trailing edge. The end supports at the trailing edge and the second web (0.90 m deep) were assumed to be pinned, while the middle support (0.60 m web) was assumed to be an elastic spring support with a stiffness equal to the in-plane stiffness of the web. The spans were 1.81 and 1.94 m, respectively.

Using the transformed section method the SNLTriax skins were transformed into the properties of the core ($n_1 = 13.65/0.256 = 53.3$) to give a transformed second moment of the 70-mm thick shell panel of $I_{t(shell)} = 5.82 \times 10^8$ mm^4. For the 600-mm deep third shear web, the SNLBiax skins were transformed to the properties of the core ($n_2 = 13.60/0.256 = 53.1$) to give a transformed second moment of the 600-mm deep web of $I_{t(web)} = 6.84 \times 10^9$ mm^4. The flexural stiffness of the shell was calculated as $E_c I_{t(shell)} = 1.49 \times 10^{11}$ N·mm^2 and that of the web $E_c I_{t(web)} = 1.75 \times 10^{12}$ N·mm^2. Solving the indeterminate structure in Fig. 6 for the contact force, R_2, between the shell and the web gave the support reactions due to factored loads, $R_1 = R_3 =$ 2,694 N, $R_2 = 2{,}876$ N. The maximum moment occurred at $x =$ 1,223 mm from S1 and was equal to $M_{max} = 1.64 \times 10^8$ N-mm. The maximum shear force was $V_{max} = 2{,}694$ N. The maximum tensile and compressive stresses in the top shell skin was $\sigma_{Triax\_skin} = \pm 5.26$ MPa and the core of $\sigma_{foam} = \pm 0.085$ MPa. The shear stress in the core was $\tau_{foam} = 2{,}694/(60)(1{,}000) = 0.045$ MPa. The downward deflection of shell due to service loads at R_2 was $\delta = 12.08$ mm.

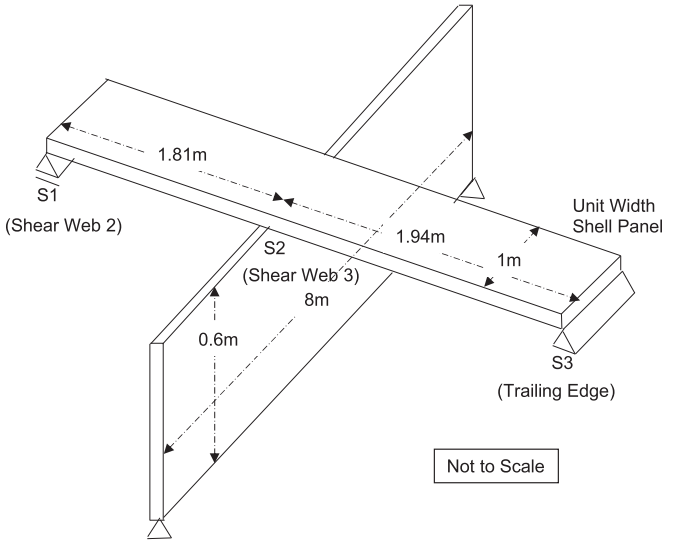

Fig. 6. Analytical model of the shell panel and supports.

In-plane Bending of the Shear Web

The 600-mm deep × 8,000-mm long web was loaded by a tributary area of half the distance (1.81 m) to SW2 on the left side and half the distance (1.94 m) to the trailing edge on the right side as shown in Fig. 7. The web was assumed to be simply supported at its two ends (spanning between the short-end walls of the house) and connected to the shell at its top edge. It was analyzed as a T-beam. The effective width of the T-beam flange was taken to be $b_{eff} = b_{web} + 16(t_{shell}) = 66 + 16(70) = 1{,}186$ mm, which is less than L/4 = 2,000 mm or the web spacing, $S = 1{,}810$ mm (ACI 318-19). For this configuration the SNLTriax skin was in its longitudinal direction and the longitudinal stiffnesses and strength properties were used: $E_{11(Triax)} = 27.7$ GPa, $\sigma_{11tens(Triax)} = +972$ MPa, $\sigma_{11comp(Triax)} = -702$ MPa. Properties of the shear web and the foam were as in Case 1.

Using the transformed section method, the SNLTriax and SNLTriax skins were transformed into the properties of the aforementioned core ($n_1 = 27.7/0.256 = 108.2$, $n_2 = 13.60/0.256 = 53.1$) giving $\bar{Y} = 589$ mm from the bottom of the web and $I_t = 2.90 \times 10^{10}$ mm^4. The uniform line load (factored) on the top of the web

was calculated to be 4.16 N/mm. The maximum bending moment at midspan assuming simple supports at the 8-m ends was $M_{max} = 3.31 \times 10^7$ N-mm, and the maximum shear force at the supports was $V_{max} = 16{,}640$ N. The maximum positive and negative flexural stresses at midspan were $\sigma_{Triax\_top} = -10.06$ MPa, $\sigma_{Biax\_bot} = +36.06$ MPa, $\sigma_{foam\_shell} = -0.087$ MPa, $\sigma_{foam\_web} = -0.680$ MPa, and $\tau_{foam\_web} = 0.462$ MPa (assuming the web foam core carries all the shear force). The maximum displacement (deflection) under service loads at midspan was 29.9 mm (span/268).

If the T-beam web is assumed to be fixed-fixed at its ends, the maximum deflection is 5.98 mm (span/1,338) and the maximum stresses at midspan (positive moment) are $\sigma_{Triax\_top} = -3.35$ MPa in the panel Triax skin and in the web Biax skin $\sigma_{Biax\_bot} = +12.01$ MPa; and the maximum stresses at the fixed support (negative moment) in the panel Triax skins, $\sigma_{Triax\_top} = +6.71$ MPa and in the web Biax skins $\sigma_{Biax\_bot} = -24.02$ MPa (all four stresses need to be determined since the section is unsymmetrical and both positive and negative moment regions exist).

Overdesign Factor—Hand Calculations

Comparing the calculated stresses and displacements to the material strengths and the code-specified deflection limits (L/240 in this case) indicates the amount of overdesign. It is important to note that this not the safety factor that is accounted for in the load and material factors used. Ideally, the structural designer attempts to get the overdesign factor (ODF) as close as possible to 1.0. In the current repurposing design the structure and its properties were predetermined by the original design (as a wind blade) and the stresses and deflections were checked with allowable values. The properties of the section cannot be changed as in a typical design iteration (although they can be modified with local stiffeners and strengtheners). The architectural design is performed at the conceptual stage where the repurposing concept is developed for different sizes of blades. Hence, the structural analysis is done to verify the acceptability of stresses and deflections, and ODFs as opposed to the safety factors need to be reported. The level of overdesign for the two aforementioned cases considered is presented separately for purposes of discussion but, in reality, the lowest number obtained is the actual ODF for the entire structure.

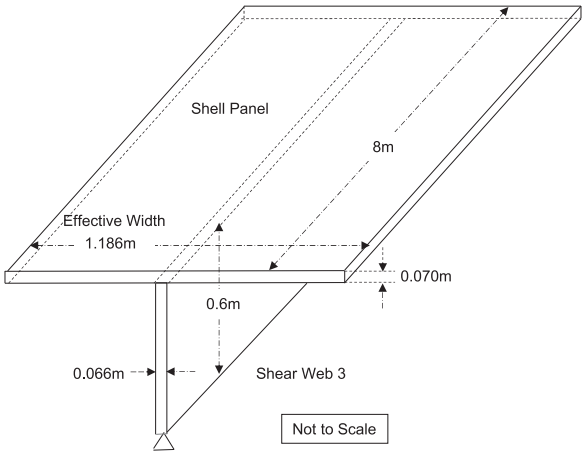

Fig. 7. Analytical model of the shear web and supports.

The calculated stresses and displacements and their relevant allowable values and ODFs for Case 1 are given in Table 2. The critical stress for the shell panel is the tensile stress in the transverse direction SNLTriax material in the top layer; but the ODF = 14.7 is high, which indicates low utilization of the material capacity. However, the deflection is closer to the code requirement with an ODF = 1.29. Since all ODFs are >1.0, the shell panel has sufficient strength and stiffness under this loading condition. For large glass fiber composite material structures, it is common that serviceability conditions control the design (Bank 2006).

The calculated stresses and displacements and their relevant allowable values and ODFs for Case 2 are given in Table 3. The critical stress for the shell panel is the tensile stress in the longitudinal direction of the SNLBiax material in the web skins, with an ODF = 2.1. The foam core critical shear stress in the web has an ODF = 2.4. Again, the serviceability condition controls the design with an ODF = 1.1. Nevertheless, all ODFs are >1.0 for these hand calculations and the structure is safe and serviceable. Note that the results given in Table 3 for the shear web are for the less conservative analysis that assumes that the shear web is pin-roller supported (as opposed to fixed-fixed) at its ends. ODFs will be higher if the fixed-fixed conditions are used.

Table 2. Hand-calculation overdesign factors (ODFs) for Case 1—shell panel

Stress or displacement component analyzed	Hand-calculated value (MPa or mm)	Relevant design property	Ultimate value (MPa or mm)	Partial safety factor (γ_M)	Code allowable (MPa or mm)	ODF = allowable/calculated values
σ_{Triax_top}	+5.26	$\sigma_{22tens(Triax)}$	+144.0	1.86	+77.4	14.7
σ_{Triax_bottom}	−5.26	$\sigma_{22comp(Triax)}$	−213.0	1.86	−114.5	21.7
σ_{foam}	+0.085	$\sigma_{tens(foam)}$	+3.1	1.86	+1.7	19.6
σ_{foam}	−0.085	$\sigma_{comp(foam)}$	−3.8	1.86	−2.0	24.0
τ_{foam}	+0.045	$\tau_{ult(foam)}$	+2.0	1.86	+1.1	23.9
$\delta_{midspan}$	12.08	L(3,650)/240	15.6	1.0	15.6	1.29

Table 3. Hand-calculation overdesign factors (ODFs) for Case 2—shear Web (T-beam)

Stress or displacement component analyzed	Hand-calculated value (MPa or mm)	Relevant design property	Ultimate value (MPa or mm)	Partial safety factor (γ_M)	Code allowable (MPa or mm)	ODF = allowable/calculated values
σ_{Triax_top}	−10.06	$\sigma_{11comp(Triax)}$	−702.0	1.86	−377.4	37.5
σ_{Biax_skin}	+36.06	$\sigma_{11tens(Biax)}$	+144.0	1.86	+77.4	2.1
σ_{foam_shell}	−0.087	$\sigma_{comp(foam)}$	−3.8	1.86	−2.0	23.0
σ_{foam_web}	−0.680	$\sigma_{comp(foam)}$	−3.8	1.86	−2.0	2.9
τ_{foam_web}	+0.462	$\tau_{ult(foam)}$	+2.0	1.86	+1.1	2.4
$\delta_{midspan}$	29.9	L(8,000)/240	33.3	1.0	33.3	1.1

Detailed Analysis—Finite Element Method

The finite element modeling of the roof was conducted using the implicit version of the LS-DYNA software code (version 4.5.21, Livermore Software Technology Corporation, Livermore, California). LS-DYNA implicit was chosen because the authors have detailed knowledge and many years of experience working with this code [both the implicit and explicit forms, e.g., Bank and Gentry (2001)]. Unfortunately, finite element codes of this type are not ideally suited to structural engineering analysis since they do not allow "automatic" evaluations of standard ASCE 7 load cases. This means that the load cases must be input manually, which is not trivial. Equally unfortunate is that standard structural engineering design codes (e.g., ETABS, STAAD, ROBOT) do not permit arbitrary laminated composite plate and shell elements.

The FEM mesh, global (X,Y,Z) and local (x,y,z) coordinate systems for the shell and the webs, and the boundary conditions are shown in Fig. 8. In Fig. 8 triangles represent pinned supports and circles roller supports, and shaded circles indicate support hidden from view in this orientation. The numbers in the model represent different layups in segments of the blade that were used in the roof. The foreshortened perspective shown in Fig. 8 is drawn looking from the 35.8 m station toward the 27.6 m station (i.e., tip to root of the blade).

Region (1) is the carbon FRP (CFRP)/glass FRP (GFRP) spar cap between Webs 1 and 2 (5 mm SNLTriax/80 mm SNLCarbon/5 mm SNLTriax), the regions (2) are the GFRP/foam shell sandwich panel (5 mm SNLTriax/60 mm foam/5 mm SNLTriax), the region (3) is the trailing edge panel (TE) (5 mm SNLTriax/15 mm Glass UD/40 mm foam/5 mm SNLTriax), and the regions (4) are the SNLBiax/foam web panels (3 mm SNLBiax/50 mm foam/3 mm SNLBiax) (Griffith 2013). A fully integrated laminated shell element (LS-DYNA ELFORM = 16) was used. The total model consisted of 3,115 nodes and 1,813 elements. The major 11-axis of the materials (Table 1) is aligned with the global Y-direction and the local x-direction for the shell and web segments (Fig. 8).

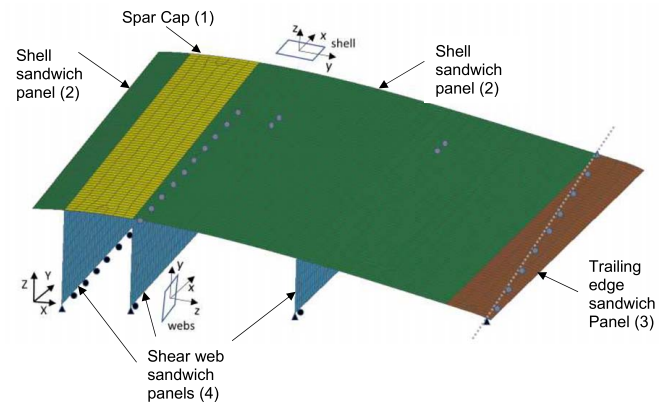

Fig. 8. FEM mesh and boundary conditions.

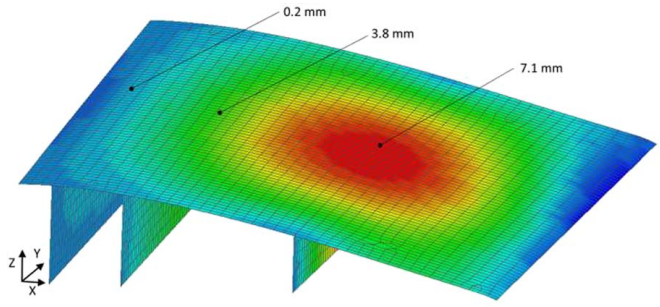

Fig. 9. Z-displacement of the roof.

Results of Finite Element Analysis

Selected results from the finite element analyses are presented to illustrate the stress distributions and displacements in key locations. As in the hand calculations, the factored load in the global Z-direction was 2.212 kN/m^2. This was uniformly distributed over the 3,115 nodes in the model. Fig. 9 shows the vertical displacement (deflection) of the roof in the negative Z-direction. The maximum displacement of 7.1 mm (downward) occurs over the third shear web near the center of the large panel between the trailing edge support and the second shear web.

The stress at the midplane of the top surface in the SNLTriax layer in the skin of the shell sandwich panel in the local y-direction is shown in Fig. 10. To help with visualization the shear webs are only shown in outline in these contour plots. The maximum compressive stress in the transverse direction of −5.0 MPa occurs in the two panels on either side of the third shear web. It can be seen that the third shear web provides a flexible intermediate support and the compressive stress decreases along this line giving the butterfly shaped stress contours. The light shading over the second shear web indicates a tensile stress and a negative curvature (and moment) over the support. Regions of high tensile stress in the shell top skin are also seen at the upper ends of the third shear web indicating negative curvature at the end of the flexible intermediate support and some fixity at the ends provided by shell action.

The stress at the midplane of the top surface in the SNLTriax layer in the skin of the shell sandwich panel in the local x-direction is shown in Fig. 11. (In this figure, the stress along the blade axis,

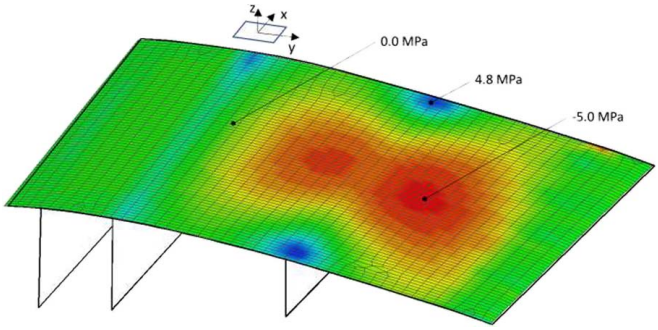

Fig. 10. Stresses in top skin layer in y-direction (blade transverse or contour direction).

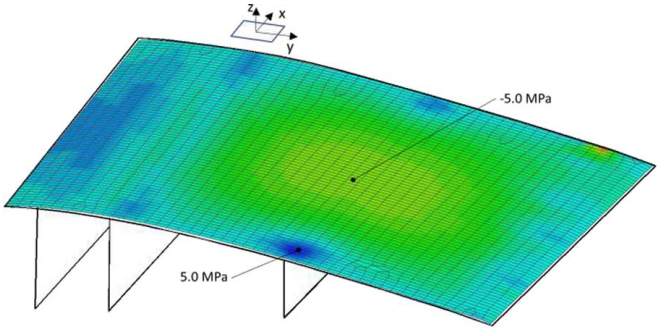

Fig. 11. Stresses in top skin layer in x-direction (blade longitudinal direction).

σ_x, is shown, while in Fig. 10 the stress transverse to the blade axis, σ_y is shown. Due to two-way bending of the panel these stresses are different.) As with the *y*-direction, the central portion is in compression (green) with a maximum longitudinal compressive stress in this region of −5.0 MPa. Similar to the *y*-direction, tensile stresses are seen in the *x*-direction at the ends of the third shear web indicating a negative curvature in this direction as well. However, this is not as significant as in the *x*-direction due to the higher stiffness of the shell skin laminate in the *x*-direction.

The displacements and stress in the shear webs are shown next. To help with visualization the shell panels are only shown in outline in these contour plots. Downward displacement of the shear webs are shown in Fig. 12. The maximum deflection in the *Z*-direction is 7.1 mm (downward) and occurs under the third shear web, which is equal to the deflection of the top shell at this location shown in Fig. 9. This to be expected as the in-plane deformation of the shear webs in the *Z*-direction is negligible. There is significantly less maximum displacement under the second shear web, which is 2.4 mm at its center. This explains the restrain provided by the second shear web and the negative curvature over the webs seen in Fig. 10. The first shear web, which is fully supported at its bottom along the wall, shows no downward displacement, as expected.

The stresses in the *x*-direction in the shear webs are shown in Fig. 13. The maximum tensile stress occurs in the SNLBiax skin in the third shear web at the bottom of the web and is equal to 10.9 MPa. Tensile stresses at the bottom of the second shear web are lower, with a maximum at the center of 5.7 MPa. It is interesting to note the relatively large compressive stresses of −25.0 MPa at the pinned supports of the shear webs. This implies a localized outward thrust due to a global restraint provided by the shell. It is important to note the shear webs are supported by roller supports (no restraint in the longitudinal *X*-direction) at their far ends (Fig. 8), so ideally there should be no thrust at the pinned supports at the near ends. However, the shear webs do not behave as simple beams and are restrained at their ends by the global two-way action of the shell.

The stresses in the local *y*-direction of the shear webs are shown in Fig. 14. Compressive stresses are noted at the supports, which are larger at the near ends due to the pinned support as noted previously.

Finally, elastic buckling analysis was conducted to check for overall instability of the roof structure. The buckling occurs at a load magnification factor of 31 (i.e., 31 × the factored load of 2.212 kN/m^2). Buckling occurs in the third shear web as is shown in Fig. 15. This is logical given the large compressive stresses seen in this location in both the local *x* and *y* directions. However, the buckling load is much larger than would be required to cause material failure in these locations and elastic instability will be precluded. Nevertheless, local stiffening will be needed at the supports of the second and third webs to prevent both local bearing failure and local buckling at these locations (Borowicz and Bank 2013).

Overdesign Factor—3-D FEM Calculations

The finite element analysis gives results for the entire structure, unlike the hand calculations where the shell and web were analyzed separately. The results for the 3-D FEM calculations are given in Table 4.

The critical stress for the roof as a whole was the compressive stress in the longitudinal direction in the SNLBiax layer in the shear web with an ODF = 4.6. All ODFs were >1.0 for this FEM analysis and the structure was safe. The critical displacement was in the shell panel with an ODF of 2.2, which satisfies serviceability requirements.

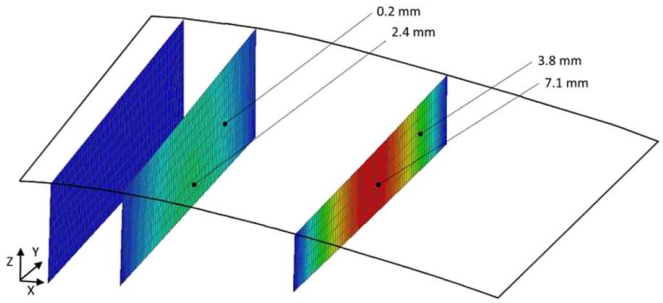

Fig. 12. Displacement of the shear webs in the *Z*-direction.

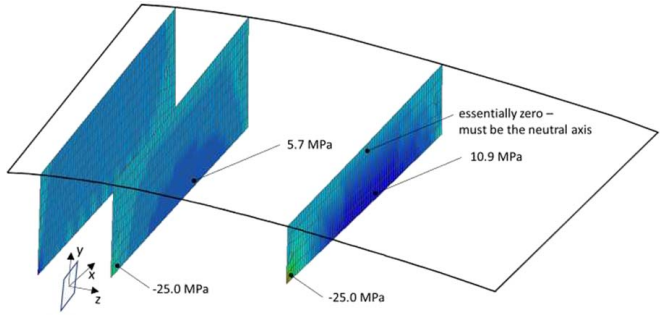

Fig. 13. Stresses in the shear webs in the *x*-direction (longitudinal direction of the web).

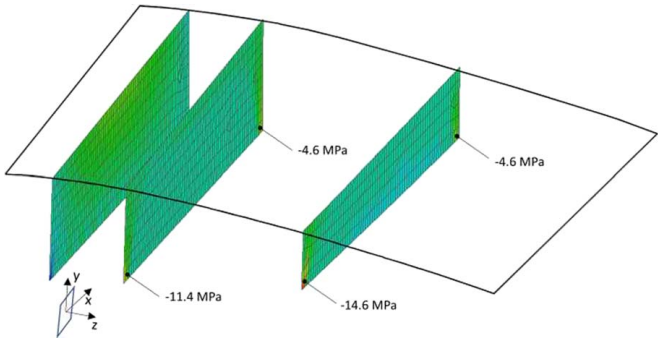

Fig. 14. Stresses in the shear webs in the *y*-direction (vertical direction in the web).

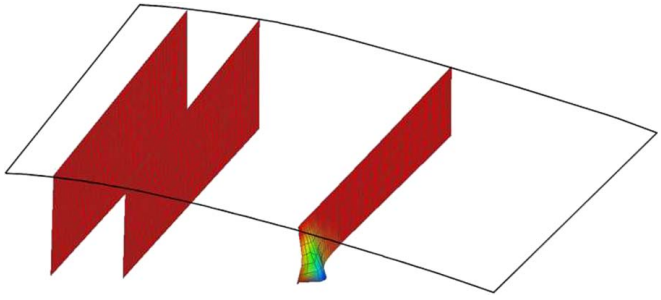

Fig. 15. Buckled shape of the third shear web.

Table 4. 3-D FEM calculation overdesign factors (ODFs) for entire roof

Stress or displacement component analyzed	Hand-calculated value (MPa or mm)	Relevant design property	Ultimate value (MPa or mm)	Partial safety factor (γ_M)	Code allowable (MPa or mm)	ODF = allowable/ calculated values
$\sigma_{y\text{Triax\_top}}$	−5.0	$\sigma_{11\text{comp(Triax)}}$	−702.0	1.86	−377.4	75.5
$\sigma_{y\text{Triax\_top}}$	+4.8	$\sigma_{11\text{tens(Triax)}}$	+972.0	1.86	+552.6	108.9
$\sigma_{x\text{Triax\_top}}$	−5.0	$\sigma_{22\text{comp(Triax)}}$	−213.0	1.86	−114.5	22.9
$\sigma_{x\text{Triax\_top}}$	+5.0	$\sigma_{22\text{tens(Triax)}}$	+144.0	1.86	+77.4	15.5
$\sigma_{x\text{Biax\_bottom}}$	+10.9	$\sigma_{11\text{tens(Biax)}}$	+144.0	1.86	+77.4	7.3
$\sigma_{x\text{Biax\_bottom}}$	−25.0	$\sigma_{11\text{comp(Biax)}}$	−213.0	1.86	−114.5	4.6
$\sigma_{y\text{Biax\_bottom}}$	−14.6	$\sigma_{22\text{comp(Biax)}}$	−213.0	1.86	−114.5	7.8
δ_{shell}	7.1	3,750/240	15.6	1.0	15.6	2.2
δ_{web}	7.1	8,000/240	33.3	1.0	33.3	4.7

Discussion

The results obtained from the one-dimensional mechanics-of-materials hand calculations and the full 3-D FEM analyses were in reasonably good agreement. Generally, the stresses and deflections obtained from the FEM analysis were less than those obtained in the hand calculations. This is to be expected as the roof shell has a two-way action that distributes loads in both the transverse and longitudinal directions. It is encouraging to know that provided good modeling assumptions are made for hand calculations, these calculations can be used in preliminary design stages to assess the feasibility of repurposing designs. In addition, the FEM analysis uncovered local multi-directional stresses, especially at the supports, which provides important input for structural detailing such as local stiffening and strengthening.

Conclusions

A methodology for structural analysis of EOL wind turbine blade sections has been developed and demonstrated. This is essential for repurposing wind turbine blades. The methodology can be applied to other structural applications for decommissioned wind turbine blades. This will contribute to improved sustainability of the wind energy sector. As indicated in the paper both hand calculations and finite element methods can be used for analysis. Nevertheless, this is not trivial, as a wind blade tapers and twists and its material properties change along its length. In either case the analysis results will only be as good as the assumptions made in building the analytical models. Over-simplification of hand-calculation models is not advised. When FEM analysis is used, laminated shell elements must be used and care must be taken to correctly orient the orthotropic materials in the laminate with respect to the global coordinate system.

For structural analysis and architectural detailing a full 3-D model showing the individual material layers of the blade is needed. However, most blade models used for aerodynamic and structural analysis are wire frame surface models. In addition, for infrastructure applications, governing building codes will need to be used since local jurisdictions permit construction based on these codes. Composite material designers are not typically familiar with these codes. At the current time a code does not exist to obtain probabilistically based material partial factors or element resistance factors for design of FRP structures. However, code-like documents can be and are used in lieu of these codes.

Data Availability Statement

Some or all data, models, or code that support the findings of this study are available from the corresponding author upon reasonable request.

Acknowledgments

Support for this research was provided by the U.S. National Science Foundation under grants 1701413 and 1701694; by InvestNI/ Department for the Economy under grant 16/US/3334; and by Science Foundation Ireland under grant USI-116 (US-Ireland Tripartite program).

References

ACI (American Concrete Institute). 2019. *2019 building code requirements for structural concrete*. ACI 318-19. Farmington Hills, MI: ACI.

3A Core Materials. 2018. "AIREX® T92.200." Accessed November 21, 2019. https://www.3accorematerials.com/en/products/airex-foam/airex-t92-pet-foam.

Adamcio, A. 2019. "Usable elements from wind turbine wings." ANMET. Accessed November 21, 2019. https://www.anmet.com.pl/.

Agarwal, B. H., L. J. Broutman, and K. Chandrashekhara. 2006. *Analysis and performance of fiber composites*. 3rd ed. Hoboken, NJ: John Wiley & Sons.

Alshannaq, A., D. Scott, L. Bank, M. Bermek, and R. Gentry. 2019. "Structural re-use of de-commissioned wind turbine blades in civil engineering applications." In *Proc., of the American Society for Composites—Thirty-Fourth Technical Conference on Composite Material*. Lancaster, Pennsylvania: DEStech Publications.

Arias, F. R. 2016. "NuMAD modeling and finite element analysis of SNL-100-01 wind turbine blade shells." B.S. thesis, Dept. of Civil Engineering, City College of New York.

Arias, F. R. 2017. "Reusing composite materials from decommissioned wind turbine blades." M.S. thesis, Dept. of Civil Engineering, City College of New York.

ASCE. 2016. *Minimum design loads and associated criteria for buildings and other structures*. ASCE 7-16. Reston, VA: ASCE.

Ascione, L., et al. 2016. *Prospect for new guidance in the design of FRP*. EUR 27666 EN. Luxembourg: Publications Office of the European Union.

Bank, L. C. 2006. *Composites for construction: Structural design with FRP materials*. Hoboken, NJ: Wiley.

Bank, L. C., F. R. Arias, T. R. Gentry, T. Al-Haddad, B. Tasistro-Hart, and J. F. Chen. 2019. "Structural analysis of FRP parts from waste wind turbine blades for building reuse applications." In *Advances in engineering materials, structures and systems: Innovations, mechanics and applications*, edited by A. Zingoni, 1520–1524. Boca Raton, FL: CRC Press.

Bank, L. C., F. R. Arias, A. Yazdanbakhsh, T. R. Gentry, T. Al-Haddad, J. F. Chen, and R. Morrow. 2018. "Concepts for reusing composite materials from decommissioned wind turbine blades in affordable housing." *Recycling* 3 (1): 3. https://doi.org/10.3390/recycling3010003.

Bank, L. C., and T. R. Gentry. 2001. "Development of a pultruded composite material highway guardrail." *Composites, Part A* 32 (9): 1329–1338. https://doi.org/10.1016/S1359-835X(01)00086-0.

Beauson, J., B. Madsen, C. Toncelli, P. Brøndsted, and J. Ilsted Bech. 2016. "Recycling of shredded composites from wind turbine blades

in new thermoset polymer composites." *Composites, Part A* 90: 390–399. https://doi.org/10.1016/j.compositesa.2016.07.009.
Berg, J. C., and B. R. Resor. 2012. *Numerical manufacturing and design tool (NuMAD v2.0) for wind turbine blades: User's guide*. SAND2012-7028. Albuquerque, NM: Sandia National Laboratories.
Bladesign. 2019. "Products." Accessed November 21, 2019. https://www.bladesign.de/products.
Borowicz, D. T., and L. C. Bank. 2013. "Effect of web reinforcement on the behavior of pultruded fiber-reinforced polymer beams subjected to concentrated loads." *Constr. Build. Mater.* 47: 347–357. https://doi.org/10.1016/j.conbuildmat.2013.05.081.
CEN (European Committee for Standardization). 1991. *Actions on structures*. Eurocode 1. Brussels, Belgium: CEN.
CEN (European Committee for Standardization). 1992. *Design of concrete structures*. Eurocode 2. Brussels, Belgium: CEN.
Directive. 2008. "Directive 2008/98/EC of the European parliament and of the council of 19 November 2008 on waste and repealing certain Directives." *Off. J. Eur. Union* 312: 3–30.
General Electric. 2019. "Haliade-x 12 MW offshore wind turbine platform." Accessed November 21, 2019. https://www.ge.com/renewableenergy/wind-energy/offshore-wind/haliade-x-offshore-turbine.
Griffith, T. 2013. *The SNL100-01 blade: Carbon design studies for the Sandia 100-meter blade*. SAND2013-1178. Albuquerque, NM: Sandia National Laboratories.
GWEC (Global Wind Energy Council). 2016. "Global wind energy outlook—2016." Accessed November 21, 2019. http://gwec.net/publications/global-wind-energy-outlook/global-wind-energy-outlook-2016/.
ICC (International Code Council). 2018. *International building code*. Washington, DC: ICC.
Jensen, J. P., and K. Skelton. 2018. "Wind turbine blade recycling: Experiences, challenges and possibilities in a circular economy." *Renewable Sustainable Energy Rev.* 97: 165–176. https://doi.org/10.1016/j.rser.2018.08.041.
Job, S., G. Leeke, P. T. Mativenga, G. Oliveux, S. Pickering, and N. A. Shuaib. 2016. "Composites Recycling: Where are we now?" Accessed November 21, 2019. https://compositesuk.co.uk/system/files/documents/Recycling%20Report%202016.pdf.
Liu, P., and C. Y. Barlow. 2017. "Wind turbine blade waste in 2050." *Waste Manage. (Oxford)* 62: 229–240. https://doi.org/10.1016/j.wasman.2017.02.007.
Mamanpush, S. H., H. Li, K. Englund, and A. T. Tabatabaei. 2018. "Recycled wind turbine blades as a feedstock for second generation composites." *Waste Manage. (Oxford)* 76: 708–714. https://doi.org/10.1016/j.wasman.2018.02.050.
Mandell, J. F., and D. D. Samborsky. 1997. *DOE/MSU composite material fatigue database. version 19.0*. Sandia Technical Rep. No. SAND97-3002. Albuquerque, NM: Sandia National Laboratories.
Oliveux, G., L. O. Dandy, and G. A. Leeke. 2015. "Current status of recycling of fibre reinforced polymers: Review of technologies, reuse and resulting properties." *Prog. Mater Sci.* 72: 61–99. https://doi.org/10.1016/j.pmatsci.2015.01.004.
Post, N. L., J. J. Lesko, and S. W. Case. 2010. "Residual strength fatigue theories for composite materials." In *Fatigue life prediction of composites and composite structures*, edited by A. P. Vassilopoulos, 79–101. Cambridge, UK: Woodhead.
Ramesh, N., T. Abbasi, S. M, S. M. Tauseefand, and S. A. Abbasi. 2018. "Utilization of fiber-reinforced plastic (FRP) waste generated by a wind-turbine manufacturing company." *Int. J. Eng. Sci. Res.* 6 (2): 103–129.
Rodin, H., S. Nassiri, K. Englund, O. Fakron, and H. Li. 2018. "Recycled glass fiber reinforced polymer composites incorporated in mortar for improved mechanical performance." *Constr. Build. Mater.* 187: 738–751. https://doi.org/10.1016/j.conbuildmat.2018.07.169.
Skelton, K. 2017. *Discussion paper on managing composite blade waste*. Brussels, Belgium: WindEurope.
SNL (Sandia National Laboratories). 2019. "SNL/MSU/DOE 2019 Composite Material Database, Version 29." Accessed November 21, 2019. https://energy.sandia.gov/programs/renewable-energy/wind-power/blade-reliability/mhk-materials-database/.
Speksnijder, S. 2018. "Reuse of wind turbine blades in a slow traffic bridge." Accessed November 21, 2019. http://www.stijnspeksnijder.com/gallery/bridge-of-blades/.
Suhail, R., J.-F. Chen, R. Gentry, B. Taristro-Hart, Y. Xue, and L. Bank. 2019. "Analysis and design of a pedestrian bridge with decommissioned FRP windblades and concrete." In *Proc., 14th Int. Symp. on Fiber-Reinforced Polymer Reinforcement of Concrete Structures*, 176. Belfast, UK: International Institute for FRP in Construction (IIFC).
SuperuseStudios. 2012. "REwind Willemsplein—Superuse Studios." Accessed November 21, 2019. https://www.superuse-studios.com/projects/rewind-willemsplein/.
Yazdanbakhsh, A., L. C. Bank, K. A. Rieder, Y. Tian, and C. Chen. 2018. "Concrete with discrete slender elements from mechanically recycled wind turbine blades." *Resour. Conserv. Recycl.* 128: 11–21. https://doi.org/10.1016/j.resconrec.2017.08.005.